INTERNAL REPORT

Statistical comparison of radio and X-ray diffuse emission in galaxy clusters

N. Pintus, F. Govoni, V. Vacca, M. Murgia,
L. Feretti, G. Giovannini, T.A. Enβlin,
F. Gastaldello, F. Cova, A. Finoguenov

Report N. 69, released: 09/10/2017

Reviewer: M. Bachetti

OAC Osservatorio Astronomico di Cagliari

Statistical comparison of radio and X-ray diffuse emission in galaxy clusters

Nicola Pintus[1], Federica Govoni[1], Valentina Vacca[1], Matteo Murgia[1], Luigina Feretti[2], Gabriele Giovannini[2,3], Torsten Enßlin[4], Fabio Gastaldello[5], Filippo Cova[5], Alexis Finoguenov[6,7]

([1]) INAF- Osservatorio Astronomico di Cagliari, Italy

([2]) INAF- Istituto di Radioastronomia di Bologna, Italy

([3]) DIFA University of Bologna, Italy

([4]) Max Planck Institut für Astrophysik, Garching, Germany

([5])INAF - IASF Milano, Italy

([6]) Max Planck Institut für Extraterrestrial Physics, Garching, Germany

([7])Department of Physics, University of Helsinki, Finland

October 9, 2017

1 Abstract

We used pointed radio observations at 1.4 GHz previously analyzed by our group in combination with archival ROSAT PSPC observations in the 0.1-2.4 keV band to perform an homogeneous analysis of the radio and X-ray surface brightness in a sample of galaxy clusters hosting cluster-wide, centrally located, diffuse synchrotron sources called radio halos. The radio and X-ray emission have been investigated both in individual clusters and globally.

2 Introduction

Clusters of galaxies, which are studied in detail by means of improved multi-wavelength telescopes, are the largest collapsed systems known so far in the Universe: since they contain information about the early Universe, they are considered the best tracers of the formation and evolution of cosmic structures.

The hot intracluster plasma of galaxy clusters reaches temperature of several million of degrees (Böhringer et al. 2002). Therefore, they are the most luminous X-ray sources in the sky ($L_X \sim 10^{44} - 10^{45}$ erg s^{-1}), comparable only to quasars ($L_X \sim 10^{43} - 10^{46}$ erg s^{-1}). For comparison, the X-ray luminosity of pulsars is of order of $L_X \sim 10^{31} - 10^{34}$ erg s^{-1}. The brightest accretion-powered X-ray pulsars show luminosities up to $L_X \sim 10^{39}$ erg s^{-1}, at the low end of the range that defines Ultraluminous X-ray sources (ULX), which are off-nuclear accreting compact objects whose X-ray luminosity (L_X 10^{39} 10^{42} erg s^{1}) exceeds the theoretical maximum for spherical infall onto stellar- mass black holes (Bachetti 2016, Israel et al. 2017).

Clusters of galaxies form from smaller subunits through several hierarchical merging processes under gravitational pull. The total energy released during cluster mergers is $\gtrsim 10^{64}$ ergs (see e.g., Sarazin 2002, Markevitch & Vikhlinin 2007), and part of this energy is dissipated through turbulent motions and shocks in the intracluster medium.

An important problem in cluster phenomenology regards large-scale diffuse radio emission not associated with individual host galaxies. Radio halos, permeating the center of galaxy clusters and extended over volumes of $\sim$1 Mpc^3, are diffuse low-surface-brightness and steep-spectrum[1] ($\alpha \gtrsim 1$) synchrotron sources with no obvious optical counterparts. They are mostly found in clusters showing evidence of merger activity suggesting a connection between the origin of radio halos and gravitational processes of cluster formation (see e.g., Feretti et al. 2012, Brunetti & Jones 2015).

A number of questions concerning the origin and evolution of radio halos are still open. There have been two competing models proposed to explain the presence of radio halos. In the turbulent re-acceleration model, seed electrons are re-energized by merger induced magnetohydrodynamical turbulence (e.g., Schlickeiser et al. 1987; Brunetti et al. 2001; Petrosian 2001; Pinzke et al. 2017). In the secondary (or hadronic) model, the cosmic ray electrons are secondary products of collisions between thermal ions and relativistic protons in the intracluster medium (e.g., Dennison 1980, Blasi &

[1] We define the radio spectrum as $S(\nu) \propto \nu^{-\alpha}$.

Colafrancesco 1999, Dolag & Enßlin 2000, Miniati et al. 2001, Pfrommer et al. 2008, Keshet & Loeb 2010; Enßlin et al. 2011; Zandanel et al. 2014).

Radio halos provide direct evidence of the presence of relativistic particles and magnetic fields associated with intra-cluster medium. They can have quite different length scales, but the largest halos are the most powerful, in such a way that all these sources may have similar synchrotron emissivity (Murgia et al. 2009). Their total radio power at 1.4 GHz strongly correlates with the cluster X-ray luminosity (Feretti 2002), temperature (Liang 1999, Colafrancesco 1999), mass (Govoni et al. 2001a), and Sunyaev-Zeldovich effect (Basu 2012) measurements.

A global analysis of radio and X-ray emission in galaxy clusters can help to discriminate between different acceleration models for cosmic rays and investigate cluster magnetic fields. Radio and X-ray properties of the clusters hosting radio halos seem to be intimately connected, and morphological similarities between radio and X-ray images have been found in a number of clusters hosting a radio halo (Govoni et al. 2001b, Storm et al. 2015). However, this similarity is generally valid for giant and regular halos. Some irregular and asymmetric halos have been found in the literature and in some cases the radio emission may show significant displacement from the X-ray emission.

A statistical investigation of the offset between the radio halo and the X-ray peak of the cluste emission pointed out that halos can be quite asymmetric with respect to the X-ray gas distribution, and this becomes more relevant when halos of smaller size are considered (Govoni et al. 2012, Feretti et al. 2012). A possible explanation for this behavior can be attributed to the cluster magnetic field power spectrum structure. Increasing the magnetic field correlation length may result in a much distorted radio halo morphology and in a significant offset of the radio halo peak from the cluster X-ray center. Smaller halos may have a more distorted morphology because they may be young systems in which the energy is still on large scales, leading to a magnetic field correlation length larger than in the more extended, and dynamically older, radio halos. The detection of polarized emission from radio halos is key to investigating the magnetic field power spectrum in galaxy clusters (Murgia et al. 2004, Govoni et al. 2006, Vacca et al. 2010, Govoni et al. 2013, Govoni et al. 2015). However, detecting this polarized signal is a very hard task and so far only three examples of large-scale filamentary polarized structures possibly associated with halo emission have been detected (Govoni et al. 2005, Bonafede et al. 2009, Girardi et al. 2016).

Following Govoni et al. (2001b) and Keshet & Loeb (2010), the purpose of this report is to perform a global radio and X-ray analysis of a sample of galaxy clusters containing giant and regular radio halos. Radio and X-ray information are obtained from pointed radio observations previously analyzed by our group, and archival ROSAT data, respectively. In Sect. 3, we present the cluster sample, the radio and X-ray data analyzed in this work, and we explain the methodology of the radio−X-ray comparison. In Sect. 4, we present the results for individual galaxy clusters. In Sect. 5, we analyze the global radio and X-ray comparison. Finally, in Sect. 6, we draw the conclusions.
Throughout this paper, we assume a ΛCDM cosmology with $H_0 = 71$ km s^{-1} Mpc^{-1}, $\Omega_m = 0.27$, and $\Omega_\Lambda = 0.73$.

3 Data analysis

Govoni et al. (2001b) established for the first time a point-to-point and a radial profile correlation between the radio and the X-ray surface brightness distribution in Coma, A2255, A2319, and A2744. While for Coma and A2255 they used available radio images at 327 MHz (Feretti & Giovannini 1998, Feretti et al. 1997a), for A2319 and A2744 they used images at 1.4 GHz (Feretti et al. 1997b, Govoni et al. 2001a). They found a linear relation ($I_{\rm RADIO} \propto I_{\rm X}^b$, with $b \simeq 1$) in the galaxy clusters A2255 and A2744 and a sub-linear (with $b < 1$) in the galaxy clusters Coma and A2319. In this report, we present a quantitative analysis of the relation between the radio and the X-ray brightness distribution for a larger sample of galaxy clusters. The radio images analyzed in this work were taken from pointed Very Large Array (VLA) or Westerbork Synthesis Radio Telescope (WSRT) observations.

Our sample consists of seven galaxy clusters (A399, A665, A2163, A2219, A2255, A2319, A2744), known to host a large scale diffuse radio halo at the cluster center. These galaxy clusters are chosen on the basis of their good radio images available in the literature at 1.4 GHz. In particular, starting from the sample of Murgia et al. (2009), we selected all the clusters characterized by a radio halo with a regular morphology, a large angular size, and with pointed ROSAT PSPC observations available in the archive. In the statistical analysis the radio images have been primary beam corrected.

The general properties of the galaxy clusters are provided in Table 1. The redshift and coordinates of each target are taken from NASA/IPAC Extragalactic Database (NED).

The X-ray images analyzed in this work were taken from archival observations carried out with the Position Sensitive Proportional Counter (PSPC) on the ROSAT satellite in the $0.1 - 2.4$ keV band. These observations are identified by their Rosat Observation Request Number (ROR) listed in Table 2. The X-ray images were corrected for the background and divided by the exposure map.

We converted from count-rate to unabsorbed flux by using the WEBPIMMS software on the HEASARC website[2]. The X-ray brightness of the clusters is well described by a thermal bremsstrahlung emission. Therefore, the conversion from count-rate to unabsorbed flux was calculated by assuming for the cluster X-ray emission an APEC model with the

[2]http://heasarc.gsfc.nasa.gov/Tools/w3pimms.html

Table 1: Sample of galaxy clusters analyzed in this work.

Cluster	RA_{J2000} (h m s)	DEC_{J2000} (d ′ ″)	z	kpc/″
A399	02 57 56.4	+13 00 59	0.0718	1.351
A665	08 30 45.2	+65 52 55	0.1819	3.030
A2163	16 15 34.1	-06 07 26	0.2030	3.306
A2219	16 40 21.4	+46 42 21	0.2256	3.588
A2255	17 12 31.0	+64 05 33	0.0806	1.501
A2319	19 21 08.8	+43 57 30	0.0557	1.068
A2744	00 14 18.9	-30 23 22	0.3080	4.502

Col. 1: Cluster name; Col. 2: Right ascension (J2000); Col. 3: Declination (J2000); Col. 4: Redshift; Col. 5 Angular to linear conversion factor.

Table 2: X-ray data of the cluster sample.

Cluster	ROR	T_{exp} [sec]	n_H [cm^{-2}]	T [kev]	Ref.	Unabs. Flux Conv. [erg/s cm^2]
A399	800235	7457	1.06×10^{21}	7.95	Cavagnolo et al. (2009)	2.384E-11
A665	800022p	38297	4.31×10^{20}	7.45	Cavagnolo et al. (2009)	1.882E-11
A2163	800385p	7096	1.08×10^{21}	19.20	Cavagnolo et al. (2009)	2.384E-11
A2219	800571p	11200	1.76×10^{20}	12.75	Cavagnolo et al. (2009)	1.473E-11
A2255	800512p	14534	2.49×10^{20}	6.12	Cavagnolo et al. (2009)	1.602E-11
A2319	800073p-1	3169	8.10×10^{20}	10.87	Cavagnolo et al. (2009)	2.223E-11
A2744	800343p	13648	1.39×10^{20}	9.18	Cavagnolo et al. (2009)	1.371E-11

Col. 1: Cluster name; Col. 2: Rosat Observation Request Number; Col 3: Exposure time; Col. 4: Galactic absorption taken from the Leiden/Argentine/Bonn (LAB) Survey of Galactic HI (Kalberla et al. 2005); Col. 5: Average cluster temperature; Col. 6: Temperature reference; Col. 7: Unabsorbed flux conversion in the 0.1-2.4 keV ROSAT band.

mean cluster temperature T, the galactic absorption n_H, and a solar abundance 0.2. We point out that in addition to the bremsstrahlung emission some other processes may contribute to a non-thermal X-ray emission. With non-thermal X-ray emission, we mean emission over that expected from the ambient cluster gas that can be approximated by a power-law (e.g. Million et al. 2009). However, a possible contribution of this non-thermal emission is negligible in the energy range $(0.1 - 2.4$ keV) analyzed in this work.

In Table 2, for each target we also show the hydrogen column density, the mean cluster temperature, the temperature reference and the conversion of the instrument count-rate into unabsorbed flux in erg s^{-1} cm^2. We used this factor conversion to pass from the X-ray surface brightness in Cts s^{-1}pixel^{-1} to erg $s^{-1}cm^{-2}$sterad^{-1}. The hydrogen column density was obtained by the n_H calculator on the HEASARC website[3]. We considered the weighted average galactic absorption n_H within a cone of radius of 1 degree from the Leiden/Argentine/Bonn (LAB) Survey of Galactic HI (Kalberla et al. 2005).

For each cluster, we investigated the radio versus the X-ray surface brightness. We converted the radio emission at 1.4 GHz from Jy/beam to erg $s^{-1}cm^{-2}$sterad^{-1} Hz^{-1} and the X-ray emission in the 0.1-2.4 KeV band from Cts s^{-1}pixel^{-2} to erg $s^{-1}cm^{-2}$sterad^{-1} by using the conversion of the instrument count-rate to the unabsorbed flux given in Table 2. We note that although the cluster temperature is known to be varying within the cluster the approximation of a mean cluster temperature does not change significantly the results. By assuming a variation ~ 2.0 keV in the cluster temperature, the resulting error in the conversion factor of counts/s into unabsorbed flux is of $\sim 0.23\%$.

4 Results on individual galaxy clusters

The brightness of the radio halos decreases with increasing distance from the cluster center, up to a radius where it fall below the sensitivity of the radio image. Although deviations of the diffuse emission from spherical symmetry are often observed, the azimuthally averaged radial profiles are indeed quite stable (Murgia et al. 2009). Since we are interested to the trend of the radio and X-ray radial surface brightness distribution, following a similar approach proposed by Govoni et al. (2001b), we calculated the mean radio and X-ray surface brightness within concentric rings centered on the cluster X-ray peak and covering the region containing the radio halo up to the $3\sigma_{RADIO}$ noise level.

The image processing was done using the Synage++ program (Murgia 2001), which allows to create concentric rings with the possibility of excluding from the statistics areas containing contaminating emission (i.e. radio and X-ray discrete

[3]https://heasarc.gsfc.nasa.gov/cgi-bin/Tools/w3nh/w3nh.pl

sources). The width of the concentric rings was chosen to obtain a good compromise between high signal to noise ratio and good resolution. We note that morphological distortions within the concentric rings do affect the profiles. In addition, since the X-ray and the radio peaks are not in general perfectly coincident, the choice of the center of the concentric rings could slightly affect the results. For each cluster of our sample, we compared the radio versus the X-ray surface brightness radial distribution. We fitted the data with a power-law relation:

$$I_{\rm RADIO} = a\, I_{\rm X}^{b} \tag{1}$$

using logarithmic units and using error-bars for both $I_{\rm RADIO}$ and $I_{\rm X}$. In addition, we graphically compared the power-law best fit, whose parameters were estimated by a least square method, with a linear ($b = 1$) relation. In the following we present the results for the individual galaxy clusters.

4.1 A399

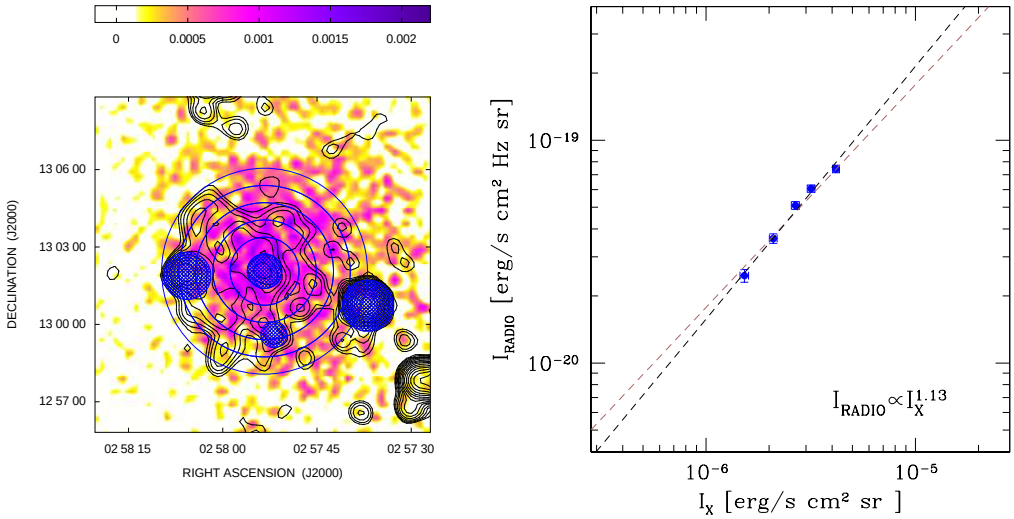

Figure 1: *Left:* The concentric rings of width 40″, used to obtain the surface brightness profiles, are overlaid on the X-ray and radio emission of A399. The cluster radio emission at 1.4 GHz with a FWHM of 45″ × 45″ is taken from Murgia et al. (2009) and is shown with contours. The first contour level is drawn at 0.12 mJy/beam and the rest are spaced by a factor of $\sqrt{2}$. The sensitivity (1σ) is 0.04 mJy/beam. The X-ray PSPC image in the 0.1-2.4 keV band is shown in colors. We indicate in blue the discrete sources excluded from the statistic. *Right:* Radio and X-ray surface brightness relation of A399. The dots show the mean of the radio and X-ray brightness obtained within each ring. The black dashed line shows the power-law best fit, while the brown dashed line indicates a linear relation with $b = 1$.

A399 and A401 represent the first example of a double radio halo in a close pair of galaxy clusters (Murgia et al. 2010). The discovery of this double halo is extraordinary given the rarity of these radio sources in general, and given that X-ray data (e.g. Sakelliou & Ponman 2004, Bourdin & Mazzotta 2008, Fujita et al. 2008), seem to suggest that the two clusters are still in a pre-merger state. In addition to the presence of the double radio halo, the *Planck* satellite, through the Sunyaev-Zel'dovich (SZ) effect, revealed a signal between the two clusters compatible with a scenario where the intercluster region is populated with a mixture of material from the clusters and the intergalactic medium, indicating that there may be a bridge of matter connecting the two systems (Planck Collaboration 2013). While the diffuse radio halo in A401 is elongated and irregular, the central region of A399 is permeated by a low-surface brightness diffuse radio halo characterized by a regular shape. A comparison between the radio and the X-ray surface brightness of A399 has never been performed. Therefore, in this report, we analyze the radio and the X-ray connection of the extended halo in A399. Although the radio halo is quite regular, Murgia et al. (2010) detected an arc-like feature of radio emission located in correspondence of a sharp X-ray edge to the east of the cluster core. No information on the radio halo spectral index are available in the literature.

We analyzed the radio and X-ray emission of A399 by averaging the surface brightness in 6 concentric rings of width 40″, centered at RA(J2000)=$02^h57^m53^s$ and DEC(J2000)=13°02′05″. Due to the presence of a radio galaxy, the central ring is not included in the statistical analysis. In the left panel of Fig.1, we show the concentric rings overlaid on the cluster X-ray and radio emission. The cluster radio emission at 1.4 GHz is taken from Murgia et al (2009) and is shown with contours. The X-ray PSPC image in the 0.1-2.4 keV band is shown in colors. The discrete sources are excluded from the statistic. In the right panel of Fig.1, we show the radio and the X-ray surface brightness comparison. The close

similarity between radio and X-ray structure is demonstrated by the correlation between these two parameters: a higher X-ray brightness is associated with a higher radio brightness. In addition these two quantities are quite well linearly correlated. The fit of the power law relation gives $b = 1.13 \pm 0.05$, and $a = -12.99 \pm 0.34$.

4.2 A665

A665 has been studied extensively at many wavelengths and it shows signs of a major merger, with a disturbed dynamical state (e.g. Markevitch & Vikhlinin 2001; Govoni et al. 2004). Recent Chandra observations of A665 (Dasadia et al. 2016) have revealed rich structures in this merging galaxy cluster, including a strong shock and two cold fronts. It is well known that the cluster of galaxies A665 contains an extended diffuse radio halo (e.g. Giovannini & Feretti 2000, Vacca et al. 2010). The radio halo is elongated in the southeast-northwest direction. The total halo flux density at 1.4 GHz is 43.1± 0.8 mJy (Giovannini & Feretti 2000), while at 327 MHz the flux density is 197 ± 6 mJy (Feretti et al. 2004). This results in an averaged spectral index of α= 1.0. Vacca et al. (2010) examined the radio halo emission in detail with deep VLA observations and constrained the cluster magnetic field power spectrum.

We analyzed the radio and X-ray connection in A665 by averaging the surface brightness in 5 concentric rings of width 50″, centered at RA(J2000)=$08^h30^m58^s$ and DEC(J2000)=65°50′40″. In the left panel of Fig.2, we show the concentric rings overlaid on the cluster X-ray and radio emission. The cluster radio emission at 1.4 GHz is taken from Vacca et al (2010) and is shown with contours. The X-ray PSPC image in the 0.1-2.4 keV band is shown in colors. The discrete sources are excluded from the statistic. In the right panel of Fig.2, we show the radio and the X-ray surface brightness comparison. In the external part of the clusters, where the radio and the X-ray surface brightness are fainter, these two parameters seems well linearly related. At the cluster center the radio brightness seems to drop. The fit of the power law relation indicates thus a sub-linear relation with $b = 0.76 \pm 0.02$ and $a = -14.76 \pm 0.08$.

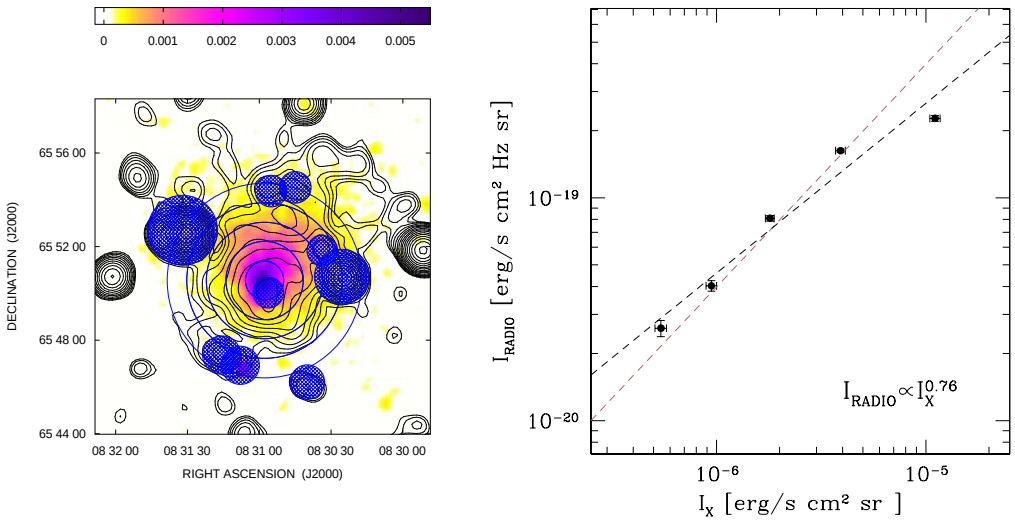

Figure 2: *Left:* The concentric rings of width 50″, used to obtain the surface brightness profiles, are overlaid on the X-ray and radio emission of A665. The cluster radio emission at 1.4 GHz with a FWHM of 55″ × 55″ is taken from Vacca et al (2010) and is shown with contours. The first contour level is drawn at 0.18 mJy/beam and the rest are spaced by a factor of $\sqrt{2}$. The sensitivity (1σ) is 0.06 mJy/beam. The X-ray PSPC image in the 0.1-2.4 keV band is shown in colors. We indicate in blue the discrete sources excluded from the statistic. *Right:* Radio and X-ray surface brightness relation of A665. The dots show the mean of the radio and X-ray brightness obtained within each ring. The black dashed line shows the power-law best fit, while the brown dashed line indicates a linear relation with $b = 1$.

4.3 A2163

The radio halo of A2163 is one of the most powerful and extended halos known so far. It shows a regular shape, slightly elongated in the E-W direction. This cluster also possesses a complex temperature structure (e.g. Markevitch & Vikhlinin 2001; Govoni et al. 2004, Bourdin et al. 2011). The presence of high-temperature gas in the cluster has been confirmed by the XMM-Newton and Chandra observations, indicating that the cluster has undergone recent merging. Feretti et al. (2001) performed a point-to-point comparison of the radio and X-ray brightness. By fitting with a power law relation, they found $b = 0.64 \pm 0.05$, indicating that the radial decline of the non-thermal radio component is slower than that of the thermal one. The total halo flux density at 1.4 GHz is 155 ± 2 mJy (Feretti et al. 2001), while at 327 MHz the flux density is 861 ± 10 mJy (Feretti et al. 2004). This leads to a total spectral index $\alpha = 1.2$.

Here, we analyzed the radio and X-ray emission of A2163 by averaging the surface brightness in 10 concentric rings of width 16″, centered at RA(J2000)=$16^h15^m46^s$ and DEC(J2000)=−06°08′43″. In the left panel of Fig.3, we show the concentric rings overlaid on the cluster X-ray and radio emission. The cluster radio emission at 1.4 GHz is taken from Feretti et al (2001) and is shown with contours. The X-ray PSPC image in the 0.1-2.4 keV band is shown in colors. The discrete sources are excluded from the statistic. In the right panel of Fig.3, we show the radio and the X-ray surface brightness comparison. The comparison between the radio emission of the halo and the cluster X-ray emission confirms a close structural similarity. The fit of the power law relation gives a relation with $b = 0.64 \pm 0.01$ and $a = -15.16 \pm 0.08$, perfectly in agreement with the previous complementary analysis by Feretti et al (2001).

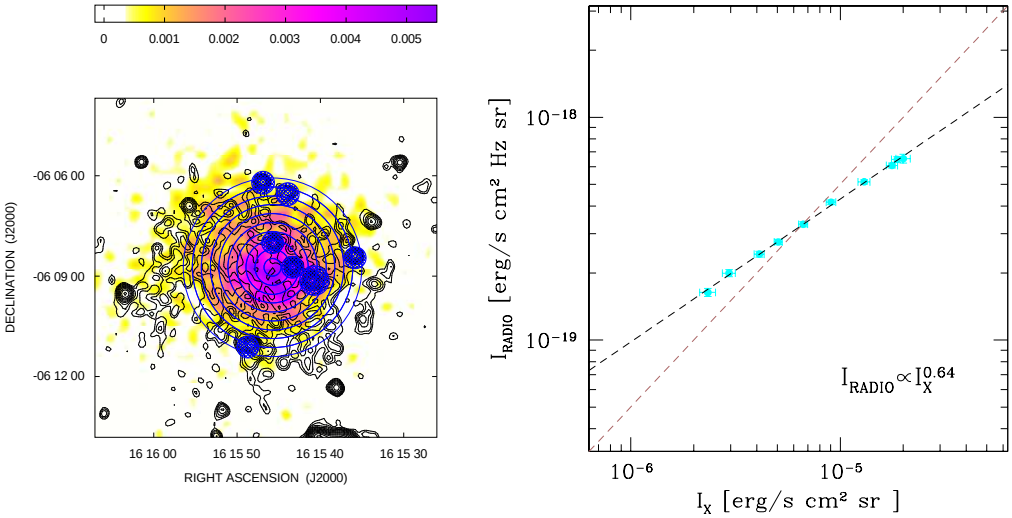

Figure 3: *Left:* The concentric rings of width 16″, used to obtain the surface brightness profiles, are overlaid on the X-ray and radio emission of A2163. The cluster radio emission at 1.4 GHz with a FWHM of 15″ × 15″ is taken from Feretti et al (2001) and is shown with contours. The first contour level is drawn at 0.09 mJy/beam and the rest are spaced by a factor of $\sqrt{2}$. The sensitivity (1σ) is 0.03 mJy/beam. The X-ray PSPC image in the 0.1-2.4 keV band is shown in colors. We indicate in blue the discrete sources excluded from the statistic. *Right:* Radio and X-ray surface brightness relation of A2163. The dots show the mean of the radio and X-ray brightness obtained within each ring. The black dashed line shows the power-law best fit, while the brown dashed line indicates a linear relation with $b = 1$.

4.4 A2219

A2219 is one of the hottest and most X-ray luminous clusters known. It is a merging system, with the dominant component of the motion in the NW-SE direction (e.g. Boschin et al. 2004, Canning et al. 2017, Million & Allen 2009). A2219 hosts a giant radio halo detected in the NVSS by Giovannini et al. (1999) and confirmed in a deeper observation at 1.4 GHz by Bacchi et al. (2003). In the cluster center there are three strong radio sources identified as cluster galaxies by Owen et al. (1992). The azimuthally averaged spectral index between 327 MHz and 1.4 GHz in the radio halo of A2219 is constant within the error, with an average value of $\alpha \simeq 1$ (Orrú et al. 2007).

We analyzed the radio and X-ray emission of A2219 by averaging the surface brightness in 7 concentric rings of width 40″, centered at RA(J2000)=$16^h40^m20^s$ and DEC(J2000)=46°42′41″. Due to the presence of radio galaxies, the two innermost rings are not included in the statistical analysis.

In the left panel of Fig.4, we show the concentric rings overlaid on the cluster X-ray and radio emission. The cluster radio emission at 1.4 GHz is taken from Bacchi et al. (2003) and is shown with contours. The X-ray PSPC image in the 0.1-2.4 keV band is shown in colors. The discrete sources are excluded from the statistic. In the right panel of Fig.4, we show the radio and the X-ray surface brightness comparison. The fit of the power law relation gives $b = 0.65 \pm 0.02$ and $a = -15.21 \pm 0.14$, indicating that the radial decline of the non-thermal radio component is slower than that of the thermal one.

4.5 A2255

A2255 is a rich cluster that shows signatures of undergoing a merger event. The cluster radio emission is characterized by a diffuse halo source at the cluster center (Jaffe & Rudnick 1979; Harris et al. 1980; Burns et al. 1995; Feretti et al. 1997a), with filaments of strong polarized emission (Govoni et al. 2005, Pizzo et al 2011). Govoni et al. (2006) examined the rotation measure of cluster radio galaxies in combination with deep VLA observations of the radio halo emission and

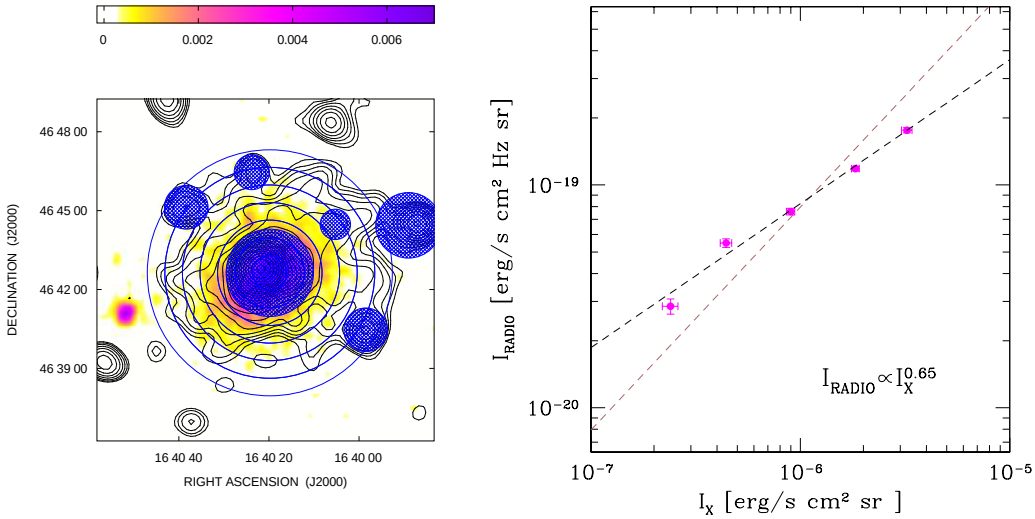

Figure 4: *Left:* The concentric rings of width 40″, used to obtain the surface brightness profiles, are overlaid on the X-ray and radio emission of A2219. The cluster radio emission at 1.4 GHz convolved with a Gaussian of a FWHM of 53″ × 53″ is taken from VLA observations by Bacchi et al (2003) and is shown with contours. The first contour level is drawn at 0.2 mJy/beam and the rest are spaced by a factor of $\sqrt{2}$. The sensitivity (1σ) is 0.07 mJy/beam. The X-ray PSPC image in the 0.1-2.4 keV band is shown in colors. We indicate in blue the discrete sources excluded from the statistic. *Right:* Radio and X-ray surface brightness relation of A2219. The dots show the mean of the radio and X-ray brightness obtained within each ring. The black dashed line shows the power-law best fit, while the brown dashed line indicates a linear relation with $b = 1$.

constrained the cluster magnetic field power spectrum. The integrated spectrum of the radio halo between 327 MHz and 1.4 GHz is $\alpha \simeq 1.7$ (Feretti et al. 1997a).

We analyzed the radio and X-ray emission of A2255 by averaging the surface brightness in 8 concentric rings of width 30″, centered at RA(J2000)=$17^h12^m44^s$ and DEC(J2000)=64°03′56″. In the left panel of Fig.5, we show the concentric rings overlaid on the cluster X-ray and radio emission. The cluster radio emission at 1.4 GHz is taken from Govoni et al. (2005) and is shown with contours. The X-ray PSPC image in the 0.1-2.4 keV band is shown in colors. The discrete sources are excluded from the statistic. In the right panel of Fig.5, we show the radio and the X-ray surface brightness comparison. These two quantities are quite well linearly correlated. The fit of the power law relation, gives $b = 1.17 \pm 0.04$ and $a = -12.22 \pm 0.23$. Govoni et al. (2001a) found a linear relation between the cluster X-ray brightness and the radio halo emission at 327 MHz.

4.6 A2319

A2319 hosts a radio halo that closely traces the cluster X-ray emission (Harris & Miley 1978, Feretti et al. 1997b, Farnsworth et al. 2013, Storm et al. 2015). The X-ray emission also reveals several signatures of merger activity (Govoni et al. 2004, O'Hara et al. 2004, Ghizzardi et al. 2010, Storm et al. 2015), including a complex temperature structure and a cold front to the SE of the central X-ray core of A2319. Some attempts to calculate a radio halo spectral index are present in the literature (e.g. Feretti et al. 1997b, Storm et al. 2015). However, this information between 327 MHz and 1.4 GHz is still missing in the literature.

We analyzed the radio and X-ray emission of A2319 by averaging the surface brightness in 11 concentric rings of width 32″, centered at RA(J2000)=$19^h21^m12^s$ and DEC(J2000)=43°56′32″. Due to the presence of a radio galaxy, the central ring is not included in the statistical analysis. In the left panel of Fig.6, we show the concentric rings overlaid on the cluster X-ray and radio emission. The cluster radio emission at 1.4 GHz is taken from Feretti et al (1997b) and is shown with contours. The X-ray PSPC image in the 0.1-2.4 keV band is shown in colors. The discrete sources are excluded from the statistic. In the right panel of Fig.6, we show the radio and the X-ray surface brightness comparison. The fit of the power law relation gives $b = 0.76 \pm 0.02$ and $a = -14.78 \pm 0.08$, in agreement within the errors with the previous point-to-point complementary analysis performed by Govoni et al. (2001). This result, who disfavors a hadronic interpretation for the radio emission (Govoni et al. 2001), is also consistent with the recent radio-Xray analysis by Storm et al. (2015).

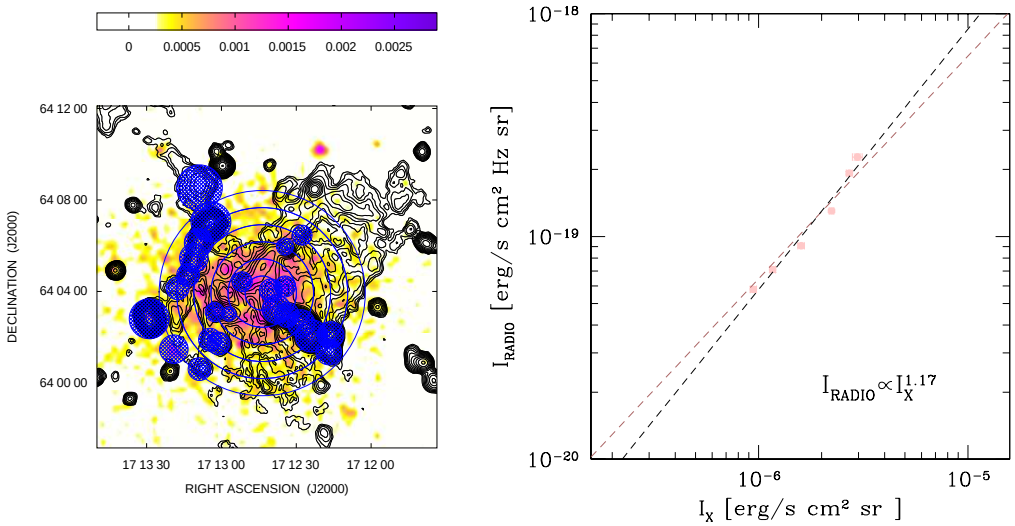

Figure 5: *Left:* The concentric rings of width 30″, used to obtain the surface brightness profiles, are overlaid on the X-ray and radio emission of A2255. The cluster radio emission at 1.4 GHz with a FWHM of 25″ × 25″ is taken from VLA observations by Govoni et al (2005) and is shown with contours. The first contour level is drawn at 0.075 mJy/beam and the rest are spaced by a factor of $\sqrt{2}$. The sensitivity (1σ) is 0.024 mJy/beam. The X-ray PSPC image in the 0.1-2.4 keV band is shown in colors. We indicate in blue the discrete sources excluded from the statistic. *Right:* Radio and X-ray surface brightness relation of A2255. The dots show the mean of the radio and X-ray brightness obtained within each ring. The black dashed line shows the power-law best fit, while the brown dashed line indicates a linear relation with $b = 1$.

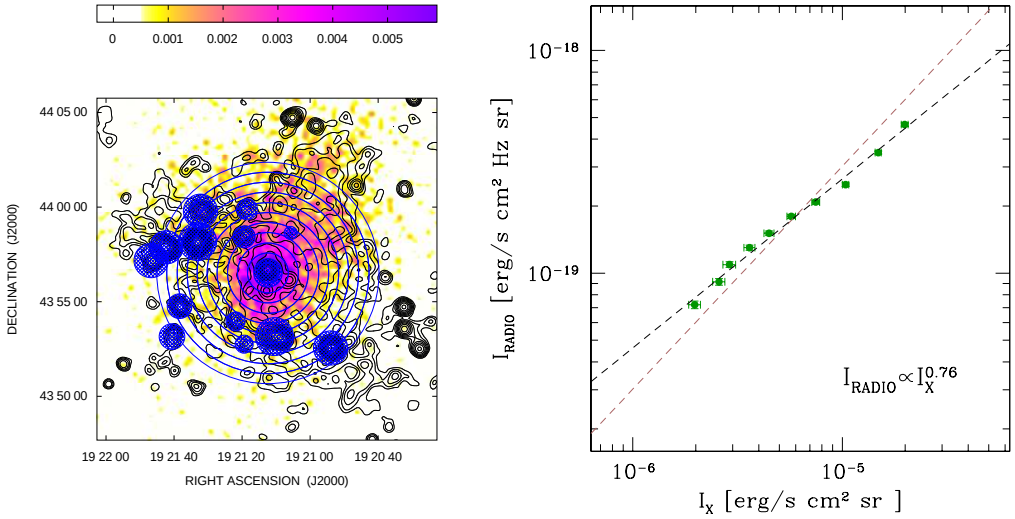

Figure 6: *Left:* The concentric rings of width 32″, used to obtain the surface brightness profiles, are overlaid on the X-ray and radio emission of A2319. The cluster radio emission at 1.4 GHz convolved with a Gaussian of a FWHM of 30″ × 30″ is taken from WSRT observations by Feretti et al (1997b) and is shown with contours. The first contour level is drawn at 0.15 mJy/beam and the rest are spaced by a factor of $\sqrt{2}$. The sensitivity (1σ) is 0.05 mJy/beam. The X-ray PSPC image in the 0.1-2.4 keV band is shown in colors. We indicate in blue the discrete sources excluded from the statistic. *Right:* Radio and X-ray surface brightness relation of A2319. The dots show the mean of the radio and X-ray brightness obtained within each ring. The black dashed line shows the power-law best fit, while the brown dashed line indicates a linear relation with $b = 1$.

4.7 A2744

A2744 hosts a central radio halo detected in the NVSS by Giovannini et al. (1999) and confirmed in a deeper observation at 1.4 GHz by Govoni et al. (2001a). Using the total flux at 327 MHz and at 1.4 GHz measured in the same area, Orrú et al. (2007) calculated an average spectral index of the halo of $\alpha \simeq 1$. Despite its regular shape, the radio halo morphology is asymmetric, being more extended toward NW. The wide X-ray emission of this cluster is characterized by the presence of substructure, which is a possible indication of a recent merger (e.g. Kempner & David 2004, Owers et al. 2011). In

particular, it is evident a sub-clump located on the NW side. Despite its regular shape, the radio halo morphology follows quite well the X-ray emission, being more extended toward NW. In addition, the radio and X-ray brightness profiles of the cluster appear to be very similar indicating that there could be an energetic relation between the X-ray thermal emitting gas and the relativistic radio emitting particles (Govoni et al. 2001a).

We analyzed the radio and X-ray emission of A2744 by averaging the surface brightness in 7 concentric rings of width 30″, centered at RA(J2000)=$00^h14^m19^s$ and DEC(J2000)=−30°23′20″. In the left panel of Fig.7, we show the concentric rings overlaid on the cluster X-ray and radio emission. The cluster radio emission at 1.4 GHz is taken from Govoni et al (2001b) and is shown with contours. The X-ray PSPC image in the 0.1-2.4 keV band is shown in colors. The discrete sources are excluded from the statistic. In the right panel of Fig.7, we show the radio and the X-ray surface brightness comparison. The radio and the X-ray emission are well related. The fit of the power law relation gives $b = 0.99 \pm 0.02$ and $a = -12.94 \pm 0.16$, indicating a linear relation between these two quantities. This result is in agreement with the previous point-to-point complementary analysis performed by Govoni et al. (2001).

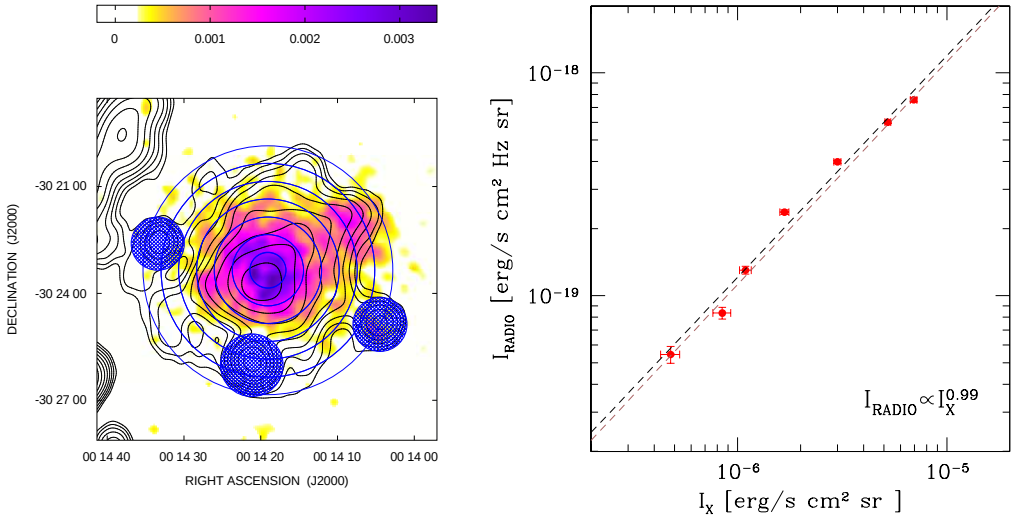

Figure 7: *Left:* The concentric rings of width 30″, used to obtain the surface brightness profiles, are overlaid on the X-ray and radio emission of A2744. The cluster radio emission at 1.4 GHz with a FWHM of 50″ × 50″ is taken from Govoni et al (2001b) and is shown with contours. The first contour level is drawn at 0.3 mJy/beam and the rest are spaced by a factor of $\sqrt{2}$. The sensitivity (1σ) is 0.1 mJy/beam. The X-ray PSPC image in the 0.1-2.4 keV band is shown in colors. We indicate in blue the discrete sources excluded from the statistic. *Right:* Radio and X-ray surface brightness relation of A2744. The dots show the mean of the radio and X-ray brightness obtained within each ring. The black dashed line shows the power-law best fit, while the brown dashed line indicates a linear relation with $b = 1$.

5 Global results

In this section we investigate the global relation between the radio and the X-ray surface brightness, by analyzing together all the clusters of our sample. This is possible since, in Sect. 4, we performed an homogeneous analysis by considering the radio halos images all obtained with pointed VLA or WSRT observations at 1.4 GHz and X-ray images all obtained with pointed ROSAT PSPC observations in the 0.1-2.4 kev band. In Fig.8, we show the global radio and the X-ray surface brightness comparison. Since the analyzed clusters are located at different redshifts ($z \simeq 0.0718 - 0.3080$), in the comparison we corrected the observed surface brightness for the cosmological dimming. As found individually, this plot confirms that in general there is a clear relation between the radio and X-ray emission of the clusters. At the cluster center an higher X-ray surface brightness is associated with an higher radio surface brightness, and these two quantities fall down by increasing the distances from the cluster center following a smooth decrease. Due to the presence of discrete radio sources blanked from the statistic, the surface brightness of central region of A339, A2219, and A2319, is not plotted in Fig.8. However, in general, the most massive and high temperature clusters like A2163, A2744, A2319 and A2219 are characterized by an higher X-ray surface brightness close to the cluster center than the less massive galaxy clusters like A2255, A665, and A399. However, this trend seems not to be perfectly reproduced in the radio emission. For example, A2163 shows the highest X-ray surface brightness but it is not the most bright in the radio band. Another interesting case is the massive galaxy cluster A2319 which shows a radio surface brightness lower than the less massive clusters A665 and A2255.

The theory behind the emission of radio halos is likely related to particle reacceleration in magnetic fields. The correlation with the X-ray data might be driven by the fact that the thermal energy of the X-ray gas is also a result of the heating by the same shocks and turbulence responsible of particle acceleration. However, the radio only traces the recent phase, while the X-ray traces the whole history. Thus, differences between the clusters could indicate the differences in the recent heating. Therefore, we can conclude that the gobal radio and X-ray relation is characterized by a significant spread that it might be due to a different content within the galaxy clusters of the magnetic fields and relativistic electrons. The investigation of the origin of this spread and the study of the magnetic field strength and relativistic particles in these clusters will be presented in a forthcoming analysis.

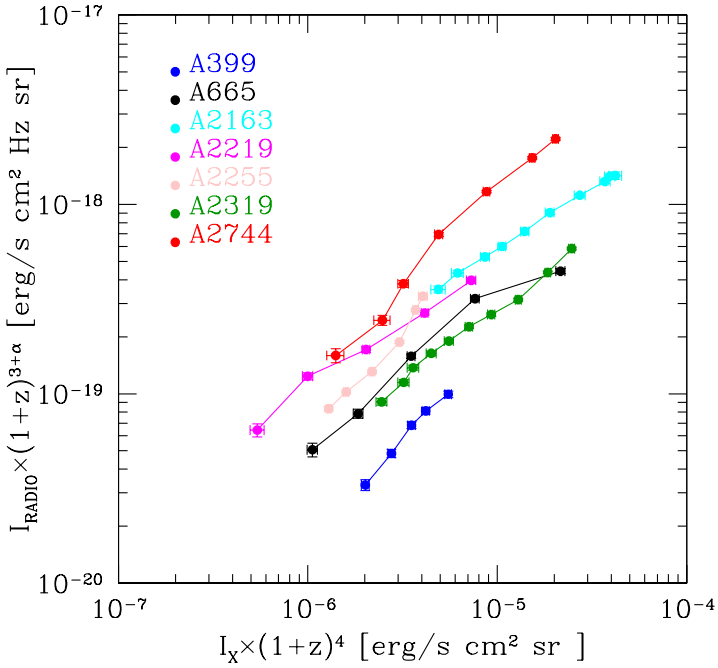

Figure 8: Radio X-ray surface brightness comparison for all the clusters analyzed in this work. The dots show the mean of the radio and X-ray brightness obtained within each ring.

6 Conclusions

We performed an homogeneous and quantitative investigation of the relation between the radio and X-ray surface brightness distribution in a sample of galaxy clusters containing a radio halo characterized by a regular morphology and a large angular size. The radio images have been all previously obtained by our group at 1.4 GHz, while in this report we took archival X-ray observations all obtained with pointed ROSAT PSPC observations in the 0.1-2.4 kev band. The cluster sample consist of the seven galaxy clusters (A399, A665, A2163, A2219, A2255, A2319, A2744) characterized by a merger activity. We analyzed these clusters both individually and globally. In Table 3 we summarize the results of the fitted power-law relation. In all the cases, a clear radio and X-ray connection is present. While in A2744, A2255, and A399 these two quantities are quite well linearly correlated, in the other cases we found a sub-linear relation between the radio and the X-ray surface brightness. This indicates that in the external part of the clusters the radio emission decreases slower than the X-ray emission.

The global radio and X-ray relation confirms the relation between the two observables. However, this relation is characterized by a significant spread which may indicate a different content within the galaxy clusters of the magnetic fields and relativistic electrons. The theoretic investigation of a linear and sub-linear relation between the radio and the X-ray emission, the origin of the spread in the global relation between clusters and the study of their magnetic field strength and relativistic particles content will be presented in a forthcoming analysis.

Acknowledgments
This research made use of the NASA/IPAC Extragalactic Database (NED), which is operated by the Jet Propulsion Laboratory, California Institute of Technology, under contract with the National Aeronautics and Space Administration.

Table 3: Results of the fitted power-law relation : $I_{\rm RADIO} = a\, I_{\rm X}^{b}$.

Cluster	a	b	χ^2_{RED}
A399	-12.99±0.34	1.13±0.05	2.4
A665	-14.76±0.08	0.76±0.02	43.5
A2163	-15.16±0.08	0.64±0.01	0.4
A2219	-15.21±0.14	0.65±0.02	8.5
A2255	-12.22±0.23	1.17±0.04	7.0
A2319	-14.78±0.08	0.76±0.02	3.2
A2744	-12.94±0.16	0.99±0.02	10.7

Col. 1: Cluster name; Col. 2: Normalization of the power-law relation; Col. 3: Exponent of the power-law relation; Col. 4: χ^2_{RED} of the fit.

7 References

Bacchi, M., Feretti, L., Giovannini, G., & Govoni, F. 2003, A&A, 400, 465

Bachetti, M. 2016, Astronomische Nachrichten, 337, 349

Basu, K. 2012, MNRAS, 421, L112

Blasi, P., & Colafrancesco, S. 1999, Astroparticle Physics, 12, 169

Böhringer, H., Schuecker, P., Guzzo, L., Collins, C. 2002, ESO Astrophysics Symposia

Bonafede, A., Feretti, L., Giovannini, G., et al., 2009, A&A, 503, 707

Boschin, W., Girardi, M., Barrena, R., et al., 2004, A&A, 416, 839

Bourdin, H., & Mazzotta, P., 2008, A&A, 479, 307

Bourdin, H., Arnaud, M., Mazzotta, P., et al., 2011, A&A, 527, A21

Brunetti, G., Setti, G., Feretti, L., Giovannini, G., 2001, MNRAS, 320, 365

Brunetti, G., & Jones, T.W., 2015, Magnetic Fields in Diffuse Media, 407, 557

Burns, J.O., Roettiger, K., Pinkney, J., et al. 1995, ApJ, 446, 583

Canning, R.E.A., Allen, S.W., Applegate, D.E., et al., 2017, MNRAS, 464, 2896

Cavagnolo, K.W., Donahue, M., Voit, G.M., Sun, M., 2009, ApJS, 182, 12

Chen, Y., Reiprich, T. H., Böhringer, H., et al., 2007, A&A, 466, 805

Colafrancesco, S., 1999, Diffuse Thermal and Relativistic Plasma in Galaxy Clusters, 269

Dasadia, S., Sun, M., Sarazin, C., et al., 2016, ApJ, 820, L20

Dennison, B., 1980, ApJ, 239, L93

Dolag, K., & Enßlin, T.A., 2000, A&A, 362, 151

Enßlin, T., Pfrommer, C., Miniati, F., Subramanian, K., 2011, A&A, 527, A99

Farnsworth, D., Rudnick, L., Brown, S., Brunetti, G., 2013, ApJ, 779, 189

Feretti, L., Boehringer, H., Giovannini, G., Neumann, D., 1997a, A&A, 317, 432

Feretti, L., Giovannini, G., Böhringer, H., 1997b, New Astronomy, 2, 501

Feretti, L., & Giovannini, G., 1998, Untangling Coma Berenices: A New Vision of an Old Cluster, Proceedings of the meeting held in Marseilles (France), June 17-20, 1997, Eds.: Mazure, A., Casoli F., Durret F., Gerbal D., Word Scientific Publishing Co Pte Ltd, p 123

Feretti, L., Fusco-Femiano, R., Giovannini, G., Govoni, F., 2001, A&A, 373, 106

Feretti, L. 2002, The Universe at Low Radio Frequencies, Pune, India, ed. A. Pramesh Rao, G. Swarup, & Gopal-Krishna, Proc. IAU Symp, 199, 133

Feretti, L., Orrù, E., Brunetti, G., et al., 2004, A&A, 423, 111

Feretti, L., Giovannini, G., Govoni, F., Murgia, M., 2012, A&A Rev., 20, 54

Fujita, Y., Tawa, N., Hayashida, K., et al., 2008, PASJ, 60, 343

Ghizzardi, S., Rossetti, M., Molendi, S., 2010, A&A, 516, A32

Giovannini, G., Tordi, M., & Feretti, L., 1999, New Astronomy, 4, 141

Giovannini, G., & Feretti, L. 2000, New Astronomy, 5, 335

Girardi, M., Boschin, W., Gastaldello, F., et al. 2016, MNRAS, 456, 2829

Govoni, F., Feretti, L., Giovannini, G., et al., 2001a, A&A, 376, 803

Govoni, F., Enßlin, T.A., Feretti, L., Giovannini, G., 2001b, A&A, 369, 441

Govoni, F., Markevitch, M., Vikhlinin, A., et al., 2004, ApJ, 605, 695

Govoni, F., Murgia, M., Feretti, L., et al., 2005, A&A, 430, L5

Govoni, F., Murgia, M., Feretti, L., et al., 2006, A&A, 460, 425

Govoni, F., Ferrari, C., Feretti, L., et al., 2012, A&A, 545, A74

Govoni, F., Murgia, M., Xu, H., et al., 2013, A&A, 554, A102

Govoni, F., Murgia, M., Xu, H., et al., 2015, Advancing Astrophysics with the Square Kilometre Array (AASKA14), 105

Harris, D.E., & Miley, G.K., 1978, A&AS, 34, 117

Harris, D.E., Kapahi, V.K., & Ekers, R.D. 1980, A&AS, 39, 215

Israel, G. L., Belfiore, A., Stella, L., et al. 2017, Science, 355, 817

Liang, H., 1999, Diffuse Thermal and Relativistic Plasma in Galaxy Clusters, 33

Kalberla, P.M.W., Burton, W. B., Hartmann, D., et al. 2005, A&A, 440, 775

Kempner, J.C., & David, L.P. 2004, MNRAS, 349, 385

Keshet, U., & Loeb, A., 2010, ApJ, 722, 737

Jaffe, W.J., & Rudnick, L., 1979, ApJ, 233, 453

Markevitch, M., & Vikhlinin, A., 2001, ApJ, 563, 95

Markevitch, M., & Vikhlinin, A., 2007, Physics Reports, 443, 1

Million, E.T., & Allen, S.W., 2009, MNRAS, 399, 1307

Miniati, F., Jones, T W., Kang, H., Ryu, D., 2001, ApJ, 562, 233

Murgia, M., 2001, Ph.D. Thesis, University of Bologna

Murgia M., Govoni F., Feretti L., et al., 2004, A&A 424, 429

Murgia, M., Govoni, F., Markevitch, M., et al., 2009, A&A, 499, 679

Murgia, M., Govoni, F., Feretti, L., Giovannini, G., 2010, A&A, 509, A86

O'Hara, T.B., Mohr, J.J., Guerrero, M.A., 2004, ApJ, 604, 604

Orrú, E., Murgia, M., Feretti, L., et al., 2007, A&A, 467, 943

Owen, F.N., White, R.A., Burns, J.O., 1992, ApJS, 80, 501

Owers, M.S., Randall, S.W., Nulsen, P.E.J., et al., 2011, ApJ, 728, 27

Ota, N., & Mitsuda, K., 2004, A&A, 428, 757

Petrosian, V., 2001, ApJ, 557, 560

Pfrommer, C., Enßlin, T.A., Springel, V., 2008, MNRAS, 385, 1211

Pinzke, A., Oh, S.P., Pfrommer, C., 2017, MNRAS, 465, 4800

Pizzo, R.F., de Bruyn, A.G., Bernardi, G., Brentjens, M.A., 2011, A&A, 525, A104

Planck Collaboration, Ade, P.A.R., Aghanim, N., et al., 2013, A&A, 550, A134

Sakelliou, I., & Ponman, T.J., 2004, MNRAS, 351, 1439

Rizza, E., Burns, J.O., Ledlow, M.J., et al., 1998, MNRAS, 301, 328

Sanderson, A.J.R., Ponman, T.J., Finoguenov, A., Lloyd-Davies, E.J., Markevitch, M., 2003, MNRAS, 340, 989

Sarazin, C.L., 2002, Merging Processes in Galaxy Clusters, ed. L. Feretti, I. M. Gioia, G. Giovannini (Kluwer Academic Publishers, Dordrecht), Astrophys. Space Sci. Lib., 272, 1

Schlickeiser, R., Sievers, A., Thiemann, H., 1987, A&A, 182, 21

Storm, E., Jeltema, T.E., & Rudnick, L., 2015, MNRAS, 448, 2495

Vacca, V., Murgia, M., Govoni, F., et al., 2010, A&A, 514, A71

Zandanel, F., Pfrommer, C., Prada, F., 2014, MNRAS, 438, 124

Zhang, Y.-Y., Böhringer, H., Finoguenov, A., et al., 2006, A&A, 456, 55

Table 4: X-ray data of some cluster of the sample.

Cluster	Obs. ID	T_{exp} [sec]	Unabs. Flux Conv. [erg/s cm^2]
A665	0109890501	132316	1.129E-11
A2163	0694500101	123818	1.556e-11
A2219	0605000501	19915	1.163E-11
A2255	0112260501	21292	1.031E-11
A2319	0600040101	58317	1.376E-11
A2744	0743850101	111900	1.065E-11

Col. 1: Cluster name; Col. 2: Observation Identifier; Col 3: Exposure time;
Col. 4: Unabsorbed flux conversion in the 0.2-12 keV XMM band.

A Appendix: A comparison with XMM profiles

In this report we used X-ray data taken from an homogeneous sample of galaxy clusters obtained with the ROSAT satellite. We are aware that more recent satellites (like Chandra and XMM) can be used for this analysis. However, ROSAT has a field of view larger than Chandra and a background more stable than XMM. To check that different satellites are expect to produce a similar X-ray profile, in this Appendix, we repeated the statistical radio X-ray comparison by using XMM data taken from the archive.

For this purpose, we analysed two clusters of our sample, namely A2163 and A2744. The methodology of this comparison is similar to that used in the rest of the report. The X-ray images were taken from observations carried out with the European Photon Imaging Camera (EPIC) on board XMM-NEWTON in the 0.2-12 keV band. These observations are identified by their Observation Identifier (Obs. ID) listed in Table 4. In Table 4 we also report the exposure time in seconds and the conversion from count-rate to unabsorbed flux obtained from the WEBPIMMS software.

In Fig. 9 we show the radio and the X-ray surface brightness profiles, both from XMM and from ROSAT PSPC, in the case of A2163 (left) and A2744 (right). We note that the XMM data are off-setted versus higher surface brightness. This is likely due to the fact that the ROSAT data are in the 0.1-2.4 keV band while the XMM data are in the 0.2-12 keV band. However, the two profiles show a very similar sub-linear relation in the case of A2163 and a linear relation for A2744, confirming the results found in this report.

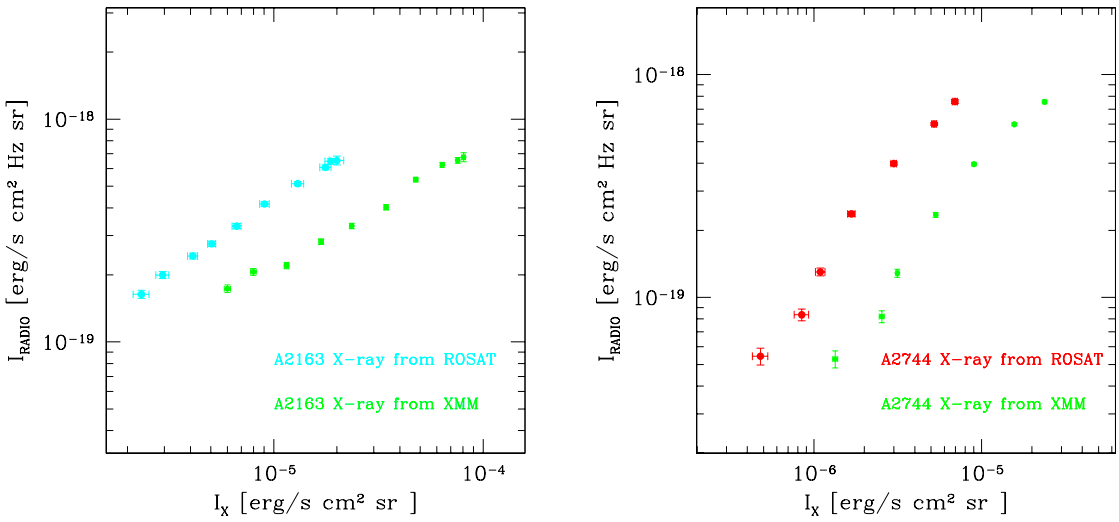

Figure 9: Radio X-ray surface brightness profile comparison for A2163 (left panel) and for A2744 (right panel) from ROSAT and XMM-NEWTON. The dots represent the mean of the radio and X-ray brightness.